

Observation of di-hadron correlations in $p^\uparrow + p$ at $\sqrt{s} = 200 \text{ GeV}$

(Dated: August 19, 2013)

We report the first significant signal from di-hadron correlations in $p^\uparrow + p$ collisions. The data were taken with the STAR detector at Brookhaven National Laboratory during the 2006 RHIC Run at $\sqrt{s} = 200$ and represent a sample of 1.8 pb^{-1} with an average beam polarization of about 60%. Di-hadron correlations are thought to originate from the fragmentation of transversely polarized quarks via the di-hadron interference fragmentation function and are thus a direct probe of the quark transversity distribution. The observed signal is the first direct transversity measurement in $p+p$ collisions.

Using the parton picture, the spin structure of the nucleon that is probed in a hard scattering process with single photon exchange and neglecting intrinsic transverse momenta, can be described by three parton distribution functions (PDFs); The unpolarized PDF $f_1(x)$, the helicity distribution function $g_1(x)$ and the so-called transversity distribution function $h_1(x)$. Here x is the lightcone momentum fraction carried by the scattered parton. In this picture $h_1(x)$ describes the probability of finding a transversely polarized parton in a transversely polarized proton. Transversity is a chiral-odd quantity and therefore, in the chiral limit of QCD and QED it is inaccessible unless it is coupled with another chiral-odd object. Transversity ~~it~~ vanishes for spin one particles, such as gluons, in spin $\frac{1}{2}$ targets like the proton because the target cannot accommodate a chirality flip which would change it by two units [1]. Until now, the only experimentally viable avenue to extract transversity has been to use transverse spin-dependent fragmentation functions as quark polarimeters. The Collins fragmentation function describes the spin dependent azimuthal distribution of single hadrons and has been used for a first extraction of transversity from a global fit to e^+e^- and SIDIS data [2]. In this paper, we analyze the spin dependence of the azimuthal distribution of hadron pairs in the final state, which is described by the di-hadron interference fragmentation function H_1^\perp (IFF) first suggested by Collins, Heppelmann and Ladinsky [3]. In contrast to the Collins Fragmentation functions, this function does not vanish upon the integration over the intrinsic transverse momenta generated in the fragmentation process, which means a collinear framework can be used for factorization and evolution. Use of a collinear framework makes the extraction of transversity independent of models for κ_T and avoids complications due to the transverse momentum dependence, such as Sudakov suppression [4, 5]. Recently the Belle experiment reported large asymmetries in di-hadron pair correlation measurements from e^+e^- annihilation [6] and the HERMES and COMPASS experiments reported large asymmetries in di-hadron correlation measurements in SIDIS, indicating that the effects are large [7, 8]. The former measurement is sensitive to the product of transverse spin-dependent fragmentation functions, whereas the latter measures transversity coupled to H_1^\perp . Experimentally, the measurement of di-

hadron correlations in polarized proton collisions, have another advantage. Since the sum and difference vectors of the two hadron momenta in the final state already allow the construction of an observable that transforms like a tensor, the reconstruction of the jet as a proxy for the fragmenting quark momentum is not necessary. Bacchetta et. al. proposed [9] to use the single spin asymmetry

$$\frac{N^\uparrow - N^\downarrow}{N^\uparrow + N^\downarrow}(\Phi_S - \Phi_R) = A_{UT}^{\sin\Phi} \sin(\Phi_S - \Phi_R). \quad (1)$$

Here, following the definition in [9], Φ_S is the angle between the polarization vector of the polarized proton to the scattering plane and Φ_R is the azimuthal angle between the difference vector between the two hadron momenta: $\vec{R} = \vec{P}_{h_1} - \vec{P}_{h_2}$ and the scattering plane. We define $\Phi_{RS} = \Phi_S - \Phi_R$ and $N^{\uparrow/\downarrow}(\Phi_{RS})$ is the number of hadron pairs in a specific angular bin when an up- or downward polarized beam hits an unpolarized target beam. At RHIC both beams are transversely polarized and the polarization pattern of the beam bunches are changed from store-to-store to reduce systematic effects. For this measurement one beam is taken as polarized and the polarization direction of the other beam is averaged over. Since the two polarization states are not equally populated, eq. 1 has to be corrected for the relative luminosity R of the two polarization states and then divided by the beam polarization P to get the intrinsic asymmetry. This leads to the relative luminosity formula:

$$A_{UT}(\Phi_{RS}) = \frac{1}{P} \frac{N^\uparrow(\Phi_{RS}) - RN^\downarrow(\Phi_{RS})}{N^\uparrow(\Phi_{RS}) + RN^\downarrow(\Phi_{RS})} \quad (2)$$

for a specific angular bin. The asymmetry of the geometric mean of particle yields in opposite sides in azimuth with opposing polarization states should lead to the same result, the so-called “cross-ratio” formula [10], with the added advantage that the relative luminosity does not have to be known

$$A_{UT}(\Phi_{RS}) = \frac{1}{P} \frac{\sqrt{N^\uparrow(\Phi_{RS})N^\downarrow(\Phi_{RS} + \pi)} - \sqrt{N^\downarrow(\Phi_{RS})N^\uparrow(\Phi_{RS} + \pi)}}{\sqrt{N^\uparrow(\Phi_{RS})N^\downarrow(\Phi_{RS} + \pi)} + \sqrt{N^\downarrow(\Phi_{RS})N^\uparrow(\Phi_{RS} + \pi)}}. \quad (3)$$

For this analysis the relative luminosity formula has been used in 16 angular bins which were then fitted with a sinusoidal function after verifying that the resulting asymmetries are consistent with the cross section calculation. For our measurement we use all charge-ordered pion pairs in the event and identify h_1 as the positive and h_2 as the negative particle. Then the amplitude $A_{UT}^{\sin\Phi}$ provides direct access to transversity, as is evident from considering the cross section for the scattering of a transversely polarized proton off an unpolarized one [9]:

$$\sigma_{UT} = 2|\vec{P}_{C\perp}| \sum_{a,b,c,d} \frac{\vec{R}}{M} |\vec{S}_T| \sin(\Phi_{RS}) \int \frac{dx_a dx_b}{16\pi z} f_1^a(x_a) h_1^b(x_b) \frac{d\Delta\sigma_{ab\uparrow\rightarrow cd\uparrow}}{d\hat{t}} H_1^{\leftarrow}(z_{\pi^+\pi^-}, M_{\pi^+\pi^-}^2). \quad (4)$$

The cross section contains a dependence on the hadron sum vector $\vec{P}_C = \vec{P}_{h_1} + \vec{P}_{h_2}$, the invariant mass $M_{\pi^+\pi^-}$ and the fractional energy with respect to the fragmenting quark $z_{\pi^+\pi^-}$ carried by the pion pair. The symbols a, b, c, d designate the partons involved in the elementary 2-2 scattering. At STAR we measure this observable using identified pion pairs in the central region of the detector where the Time Projection Chamber (TPC) provides reliable tracking and charged pion identification [11]. The analyzed dataset represents an integrated luminosity of 1.8 pb^{-1} collected in 2006 during RHIC run 6, with an average polarization of about 60% for each beam. Most events are triggered by requiring at least 4 or 7.8 GeV transverse energy E_T in a 1.0×1.0 jet patch in the barrel electromagnetic calorimeter (BEMC) or at least 5 GeV E_T in a single BEMC tower. In addition, a coincidence between two forward segmented scintillators placed at $3.3 < \eta < 5.0$ on either side of the interaction point was required. The bias in sampling the underlying event kinematics with these triggers is illustrated in fig. 6, which shows the change of the mean x obtained from a Pythia simulation in each $p_{T_{\pi^+\pi^-}}$ bin after the trigger condition is applied. Charged pion pairs are selected by requiring tracks that originate within 60 cm in the z direction and 1 cm in the transverse direction from the nominal interaction vertex and that point into the barrel. Tracks were required to have a minimum transverse momentum p_T of 1.5 GeV/c and using dE/dx a purity of the single pion sample of greater than 95% over the whole kinematic range is achieved. All pion pairs in an event are considered where the pions are close enough in $(\eta - \phi)$ space to originate from the fragmentation of the same parton. The default value of this ‘‘cone cut’’ is $\sqrt{(\eta_{\pi_1} - \eta_{\pi_2})^2 + (\phi_{\pi_1} - \phi_{\pi_2})^2} < 0.3$. Pion pairs in the invariant mass range of the K^0 (497.6+- 10 MeV) were excluded.

Figure 1 shows the results for $A_N^{\sin\phi}$ binned in the invariant mass $M_{\pi^+\pi^-}$ of the hadron pair separately for particles going in the forward and backward direction

($\eta_{\pi^+\pi^-} \lesssim 0$) where $\eta_{\pi^+\pi^-}$ is the pseudorapidity of the pion pair with respect to the polarized beam.

A clear signal is seen in the forward direction around the ρ mass. From model calculations this is expected since the observed effect originates from the interference of amplitudes with different angular momenta [12]; mainly this will be pions in a relative p-wave from vector meson decays interfering with pions in a relative s-wave from the non-resonant background. In addition to the s-p interference, contributions from p-p interference are possible at our kinematics. However the p-p contribution is proportional to $\cos\theta$ whereas the s-p interference term is proportional to $\sin\theta$, with θ being the decay angle in the two-hadron center of mass frame. For this measurement, the average $\sin\theta$ value in each kinematic bin is close to unity and conversely the $\cos\theta$ distribution has a mean of zero. Therefore only the s-p contribution is of relevance. Figure 2 also shows significant asymmetries at large transverse momenta of the hadron pair $p_{T_{\pi^+\pi^-}}$ where the contribution from valence quarks is enhanced. Backward asymmetries which would be sensitive to quarks at small x are small, as is expected if transversity is mainly carried by the valence quarks. We also investigated the effect of different cone cuts from 0.2 up to 0.4 as shown in fig. 3 and 4. As $z_{\pi^+\pi^-}$, the mean $p_{T_{\pi^+\pi^-}}$ and $M_{\pi^+\pi^-}$, respectively are dependent on the size of the cone, larger cone sizes allowing for more pions at low transverse momenta and low $z_{\pi^+\pi^-}$, we can observe the combined $p_{T_{\pi^+\pi^-}}$, $M_{\pi^+\pi^-}$ dependence of the asymmetries. At fixed $M_{\pi^+\pi^-}$, the asymmetries reflect the $p_{T_{\pi^+\pi^-}}$ dependence for different cone cuts, whereas the asymmetries at fixed $p_{T_{\pi^+\pi^-}}$ have no strong dependence on the cone cut which is consistent with our simulations which indicate very little variation of x and $z_{\pi^+\pi^-}$. Figure 5 shows the $\eta_{\pi^+\pi^-}$ dependence which, in turn, reflects the x dependence of transversity. Higher values of $\eta_{\pi^+\pi^-}$ probe higher x where the magnitude of h_1 is larger. Consistent with this expectation the asymmetries rise with $\eta_{\pi^+\pi^-}$. The leading systematic uncertainty for our results comes from the 4.8% scale uncertainty on the beam polarization. The purity in the single pion sample averages to 96%. There is a mild p_T dependence with purities ranging from 94% for low p_T bins to 97% for high p_T bins. The resulting dilution of the analyzed hadron pair sample with $\pi - K$ pairs was not used in assigning a systematic error due to the unknown size of the $\pi - K$ signal. There are however, hints [13] that these asymmetries are of similar or smaller magnitude than the $\pi^+\pi^-$ and of the same sign.

In summary, STAR has detected the first signal of transversity in $p^\uparrow + p$ collisions. We observed significant asymmetries around the ρ invariant mass that rise with $p_{T_{\pi^+\pi^-}}$ and $\eta_{\pi^+\pi^-}$ consistent with qualitative expectations from the transversity distribution function and the IFF. These results can be included in the point-by-point extractions of transversity in a collinear framework that

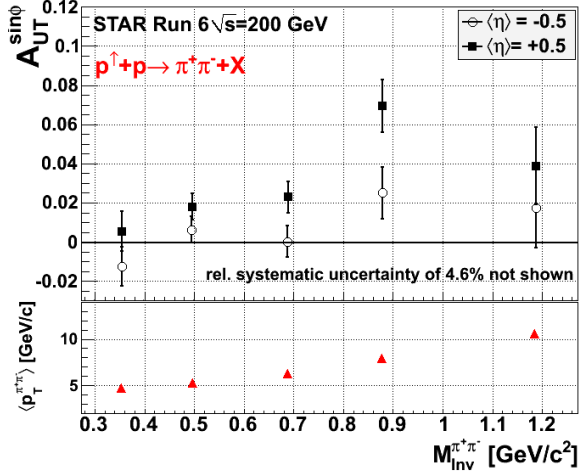


FIG. 1. $A_N^{\sin\phi}$ as a function of $M_{\pi^+\pi^-}$ (left) and $p_{T_{\pi^+\pi^-}}$. A clear enhancement of the signal around the ρ mass region can be observed and only the largest transverse momenta contribute to the asymmetry.

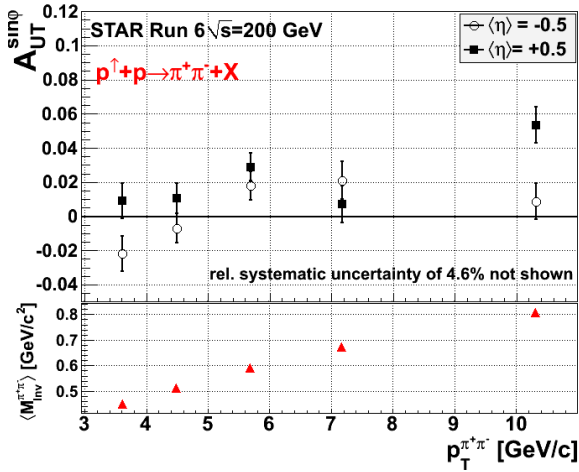


FIG. 2. $A_N^{\sin\phi}$ as a function of $p_{T_{\pi^+\pi^-}}$. Only the largest transverse momenta contribute to the asymmetry.

are currently underway [14]. Compared with previous measurements of di-hadron correlations in semi-inclusive deep inelastic scattering (SIDIS), the RHIC data allows access to a complementary kinematic regime and proton-proton collisions do not suffer from u-quark dominance and will therefore help constrain, in particular, the d-quark transversity. A large dataset taken in 2012 will allow us to reduce the error bars on this measurement by about a factor of 3 and hadron pairs involving neutral pions will be investigated.

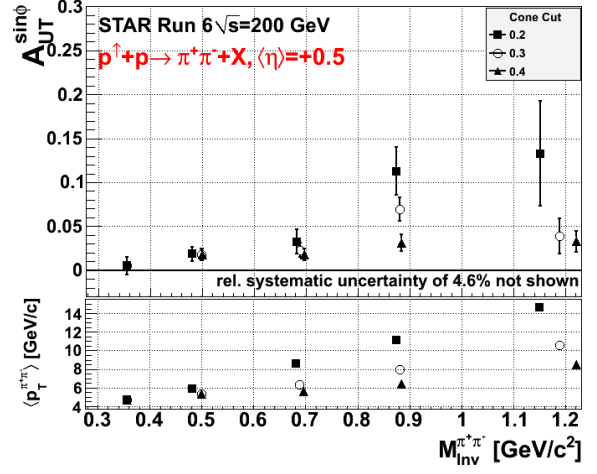


FIG. 3. $A_N^{\sin\phi}(M_{\pi^+\pi^-})$ with different cone cuts. The signal in each $M_{\pi^+\pi^-}$ bin exhibits a strong dependence on the mean $p_{T_{\pi^+\pi^-}}$. Data points are offset for visibility.

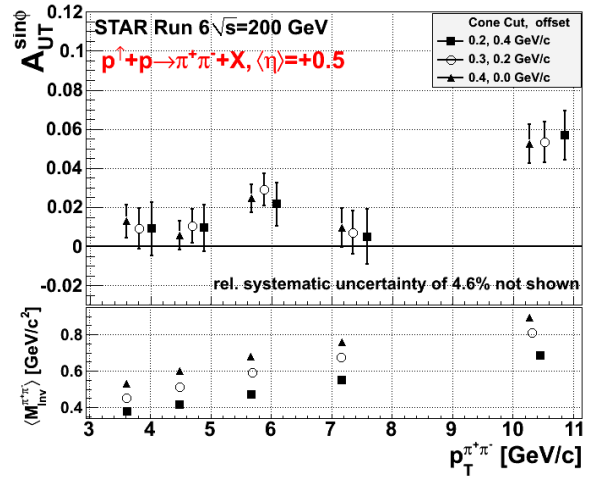


FIG. 4. $A_N^{\sin\phi}(p_{T_{\pi^+\pi^-}})$ with different cone cuts. In a given $p_{T_{\pi^+\pi^-}}$ bin the dependence on the cone cut and thus on the mean $M_{\pi^+\pi^-}$ is only weak. Data points are offset for visibility.

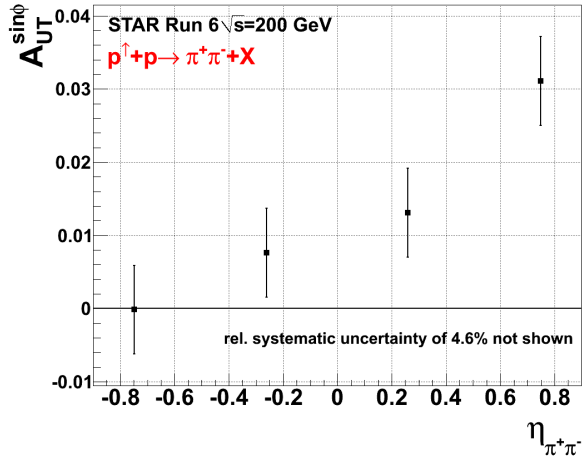


FIG. 5. $A_N^{\sin\phi}$ as a function of $\eta_{\pi^+\pi^-}$. The strong dependence of the asymmetries on the pseudo-rapidity reflects the x dependence of transversity.

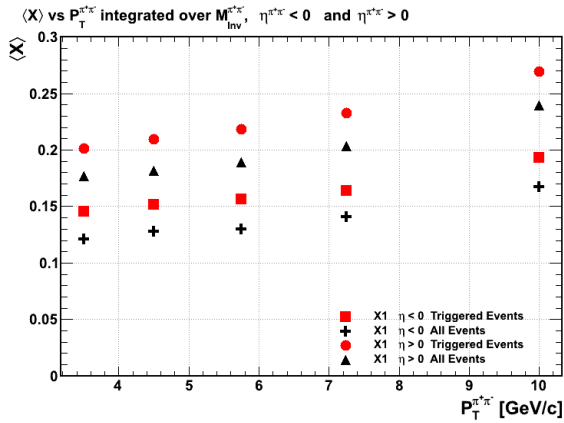


FIG. 6. Change of the mean x obtained from a Pythia simulation in each $p_{T,\pi^+\pi^-}$ bin after the trigger condition is applied for positive and negative values of $\eta_{\pi^+\pi^-}$.

-
- [1] V. Barone, A. Drago, and P. G. Ratcliffe, Phys.Rept. **359**, 1 (2002), arXiv:hep-ph/0104283 [hep-ph].
 - [2] M. Anselmino, M. Boglione, U. D'Alesio, A. Kotzinian, F. Murgia, *et al.*, Phys.Rev. **D75**, 054032 (2007), arXiv:hep-ph/0701006 [hep-ph].
 - [3] J. C. Collins, S. F. Heppelmann, and G. A. Ladinsky, Nucl.Phys. **B420**, 565 (1994), arXiv:hep-ph/9305309 [hep-ph].
 - [4] A. Bianconi, S. Boffi, R. Jakob, and M. Radici, Phys.Rev. **D62**, 034008 (2000), arXiv:hep-ph/9907475 [hep-ph].
 - [5] A. Bacchetta, (2002), arXiv:hep-ph/0212025 [hep-ph].
 - [6] A. Vossen *et al.* (Belle Collaboration), Phys.Rev.Lett. **107**, 072004 (2011), arXiv:1104.2425 [hep-ex].
 - [7] A. Airapetian *et al.* (HERMES Collaboration), JHEP **0806**, 017 (2008), arXiv:0803.2367 [hep-ex].
 - [8] C. Adolph *et al.* (COMPASS Collaboration), Phys.Lett. **B713**, 10 (2012), arXiv:1202.6150 [hep-ex].
 - [9] A. Bacchetta and M. Radici, Phys.Rev. **D70**, 094032 (2004), arXiv:hep-ph/0409174 [hep-ph].
 - [10] G. G. Ohlsen and P. W. Keaton, Nucl. Instrum. Meth. **109** (1973).
 - [11] K. Ackermann *et al.* (STAR Collaboration), Nucl.Instrum.Meth. **A499**, 624 (2003).
 - [12] A. Bianconi, S. Boffi, R. Jakob, and M. Radici, Phys.Rev. **D62**, 034009 (2000), arXiv:hep-ph/9907488 [hep-ph].
 - [13] C. Braun (presented at the workshop Structure of Nucleons and Nuclei, Como, 10-14 June, 2013).
 - [14] A. Bacchetta, A. Courtoy, and M. Radici, Phys. Rev. Lett. **107**, 012001 (2011).

SUPPLEMENTAL INFORMATION

TABLE I. $p_T^{\pi^+\pi^-}$ asymmetries, $\eta^{\pi^+\pi^-} < 0$, cone cut of 0.2

$\langle p_T^{\pi^+\pi^-} \rangle$ [GeV/c]	$\langle \sin \theta \rangle$	$\langle M_{\text{Inv}}^{\pi^+\pi^-} \rangle$ [GeV]	$A_{\text{UT}}^{\sin \phi}$	$\sigma_{A_{\text{UT}}^{\sin \phi}}$	$\langle z \rangle$	$\langle x_1 \rangle$	$\langle x_2 \rangle$	$\langle \eta^{\pi^+\pi^-} \rangle$
3.62	0.99	0.38	-0.0307	0.0138	0.29	0.15	0.20	-0.50
4.49	0.96	0.41	-0.0100	0.0119	0.35	0.15	0.20	-0.51
5.70	0.93	0.47	0.0229	0.0110	0.44	0.16	0.21	-0.51
7.18	0.91	0.55	0.0159	0.0140	0.48	0.16	0.23	-0.51
10.45	0.88	0.68	0.0085	0.0125	0.57	0.17	0.23	-0.51

TABLE II. $\langle M_{\text{Inv}}^{\pi^+\pi^-} \rangle$ asymmetries, $\eta^{\pi^+\pi^-} < 0$, cone cut of 0.2

$\langle M_{\text{Inv}}^{\pi^+\pi^-} \rangle$ [GeV]	$\langle \sin \theta \rangle$	$\langle p_T^{\pi^+\pi^-} \rangle$ [GeV/c]	$A_{\text{UT}}^{\sin \phi}$	$\sigma_{A_{\text{UT}}^{\sin \phi}}$	$\langle z \rangle$	$\langle x_1 \rangle$	$\langle x_2 \rangle$	$\langle \eta^{\pi^+\pi^-} \rangle$
0.36	0.95	4.73	-0.0125	0.0101	0.38	0.16	0.22	-0.51
0.48	0.94	5.93	0.0145	0.0080	0.43	0.16	0.22	-0.51
0.68	0.91	8.58	-0.0044	0.0140	0.53	0.17	0.24	-0.51
0.88	0.90	11.13	0.0224	0.0272	0.59	0.21	0.28	-0.51
1.15	0.90	14.57	0.0042	0.0617	0.63	0.23	0.34	-0.49

TABLE III. $p_T^{\pi^+\pi^-}$ asymmetries, $\eta^{\pi^+\pi^-} > 0$, cone cut 0.2

$\langle p_T^{\pi^+\pi^-} \rangle$ [GeV/c]	$\langle \sin \theta \rangle$	$\langle M_{\text{Inv}}^{\pi^+\pi^-} \rangle$ [GeV]	$A_{\text{UT}}^{\sin \phi}$	$\sigma_{A_{\text{UT}}^{\sin \phi}}$	$\langle z \rangle$	$\langle x_1 \rangle$	$\langle x_2 \rangle$	$\langle \eta^{\pi^+\pi^-} \rangle$
3.62	0.99	0.38	0.0090	0.0138	0.28	0.21	0.15	0.50
4.49	0.96	0.41	0.0095	0.0118	0.34	0.21	0.15	0.51
5.70	0.93	0.47	0.0216	0.0110	0.42	0.22	0.15	0.95
7.18	0.91	0.55	0.0050	0.0139	0.50	0.23	0.16	0.95
10.45	0.88	0.68	0.0568	0.0124	0.58	0.27	0.20	0.94

TABLE IV. $\langle M_{\text{Inv}}^{\pi^+\pi^-} \rangle$ asymmetries, $\eta^{\pi^+\pi^-} > 0$, cone cut 0.2

$\langle M_{\text{Inv}}^{\pi^+\pi^-} \rangle$ [GeV]	$\langle \sin \theta \rangle$	$\langle p_T^{\pi^+\pi^-} \rangle$ [GeV/c]	$A_{\text{UT}}^{\sin \phi}$	$\sigma_{A_{\text{UT}}^{\sin \phi}}$	$\langle z \rangle$	$\langle x_1 \rangle$	$\langle x_2 \rangle$	$\langle \eta^{\pi^+\pi^-} \rangle$
0.36	0.95	4.73	0.0054	0.0101	0.38	0.23	0.16	0.51
0.48	0.94	5.93	0.0189	0.0081	0.42	0.22	0.16	0.94
0.68	0.91	8.58	0.0328	0.0139	0.55	0.25	0.17	0.94
0.88	0.90	11.13	0.1128	0.0274	0.60	0.27	0.20	0.51
1.15	0.90	14.57	0.1328	0.0598	0.65	0.31	0.24	0.48

TABLE V. $p_T^{\pi^+\pi^-}$ asymmetries, $\eta^{\pi^+\pi^-} < 0$, cone cut 0.3

$\langle p_T^{\pi^+\pi^-} \rangle$ [GeV/c]	$\langle \sin \theta \rangle$	$\langle M_{\text{Inv}}^{\pi^+\pi^-} \rangle$ [GeV]	$A_{\text{UT}}^{\sin \phi}$	$\sigma_{A_{\text{UT}}^{\sin \phi}}$	$\langle z \rangle$	$\langle x_1 \rangle$	$\langle x_2 \rangle$	$\langle \eta^{\pi^+\pi^-} \rangle$
3.61	0.99	0.45	-0.0220	0.0103	0.30	0.15	0.20	0.97
4.49	0.97	0.51	-0.0070	0.0087	0.36	0.15	0.20	0.94
5.68	0.94	0.59	0.0179	0.0082	0.43	0.16	0.22	0.92
7.17	0.92	0.67	0.0211	0.0110	0.48	0.16	0.23	0.88
10.32	0.88	0.81	0.0088	0.0106	0.57	0.19	0.27	0.88

TABLE VI. $\langle M_{\text{Inv}}^{\pi^+\pi^-} \rangle$ asymmetries, $\eta^{\pi^+\pi^-} < 0$, cone cut 0.3

$\langle M_{\text{Inv}}^{\pi^+\pi^-} \rangle$ [GeV]	$\langle \sin \theta \rangle$	$\langle p_T^{\pi^+\pi^-} \rangle$ [GeV/c]	$A_{\text{UT}}^{\sin \phi}$	$\sigma_{A_{\text{UT}}^{\sin \phi}}$	$\langle z \rangle$	$\langle x_1 \rangle$	$\langle x_2 \rangle$	$\langle \eta^{\pi^+\pi^-} \rangle$
0.36	0.95	4.73	-0.0125	0.0101	0.38	0.16	0.22	0.92
0.50	0.95	5.35	0.0063	0.0068	0.41	0.16	0.21	0.94
0.69	0.94	6.35	0.0002	0.0081	0.44	0.16	0.22	0.92
0.88	0.92	7.98	0.0250	0.0134	0.50	0.17	0.25	0.90
1.19	0.90	10.63	0.0172	0.0200	0.56	0.19	0.27	0.90

TABLE VII. $p_T^{\pi^+\pi^-}$ asymmetries, $\eta^{\pi^+\pi^-} > 0$, cone cut 0.3

$\langle p_T^{\pi^+\pi^-} \rangle$ [GeV/c]	$\langle \sin \theta \rangle$	$\langle M_{\text{Inv}}^{\pi^+\pi^-} \rangle$ [GeV]	$A_{\text{UT}}^{\sin \phi}$	$\sigma_{A_{\text{UT}}^{\sin \phi}}$	$\langle z \rangle$	$\langle x_1 \rangle$	$\langle x_2 \rangle$	$\langle \eta^{\pi^+\pi^-} \rangle$
3.61	0.99	0.45	0.0092	0.0103	0.29	0.20	0.14	0.51
4.49	0.97	0.51	0.0106	0.0086	0.35	0.21	0.15	0.51
5.68	0.94	0.59	0.0289	0.0082	0.43	0.22	0.15	0.94
7.17	0.92	0.67	0.0071	0.0110	0.50	0.23	0.16	0.92
10.32	0.88	0.81	0.0533	0.0106	0.58	0.27	0.19	0.88

TABLE VIII. $\langle M_{\text{Inv}}^{\pi^+\pi^-} \rangle$ asymmetries, $\eta^{\pi^+\pi^-} > 0$, cone cut 0.3

$\langle M_{\text{Inv}}^{\pi^+\pi^-} \rangle$ [GeV]	$\langle \sin \theta \rangle$	$\langle p_T^{\pi^+\pi^-} \rangle$ [GeV/c]	$A_{\text{UT}}^{\sin \phi}$	$\sigma_{A_{\text{UT}}^{\sin \phi}}$	$\langle z \rangle$	$\langle x_1 \rangle$	$\langle x_2 \rangle$	$\langle \eta^{\pi^+\pi^-} \rangle$
0.36	0.95	4.73	0.0054	0.0101	0.38	0.23	0.16	0.51
0.48	0.94	5.93	0.0189	0.0081	0.42	0.22	0.16	0.94
0.68	0.91	8.58	0.0328	0.0139	0.55	0.25	0.17	0.94
0.88	0.90	11.13	0.1128	0.0274	0.60	0.27	0.20	0.51
1.19	0.90	14.57	0.1328	0.0598	0.65	0.31	0.24	0.48

TABLE IX. $p_T^{\pi^+\pi^-}$ asymmetries, $\eta^{\pi^+\pi^-} < 0$, cone cut 0.4

$\langle p_T^{\pi^+\pi^-} \rangle$ [GeV/c]	$\langle \sin \theta \rangle$	$\langle M_{\text{Inv}}^{\pi^+\pi^-} \rangle$ [GeV]	$A_{\text{UT}}^{\sin \phi}$	$\sigma_{A_{\text{UT}}^{\sin \phi}}$	$\langle z \rangle$	$\langle x_1 \rangle$	$\langle x_2 \rangle$	$\langle \eta^{\pi^+\pi^-} \rangle$
3.61	0.99	0.45	-0.0161	0.0084	0.30	0.14	0.20	-0.51
4.49	0.97	0.51	-0.0081	0.0073	0.36	0.15	0.20	-0.51
5.68	0.94	0.59	0.0130	0.0073	0.43	0.15	0.21	-0.51
7.17	0.92	0.67	0.0163	0.0101	0.48	0.16	0.24	-0.51
10.28	0.88	0.89	0.0148	0.0099	0.57	0.19	0.27	-0.51

TABLE X. $\langle M_{\text{inv}}^{\pi^+\pi^-} \rangle$ asymmetries, $\eta^{\pi^+\pi^-} < 0$, cone cut 0.4

$\langle M_{\text{inv}}^{\pi^+\pi^-} \rangle$	$\langle \sin \theta \rangle$	$\langle p_T^{\pi^+\pi^-} \rangle$ [GeV/c]	$A_{\text{UT}}^{\sin \phi}$	$\sigma_{A_{\text{UT}}^{\sin \phi}}$	$\langle z \rangle$	$\langle x_1 \rangle$	$\langle x_2 \rangle$	$\langle \eta^{\pi^+\pi^-} \rangle$
0.36	0.95	4.73	-0.0125	0.0101	0.38	0.16	0.22	0.36
0.50	0.95	5.31	0.0054	0.0067	0.41	0.16	0.21	0.50
0.70	0.96	5.60	-0.0022	0.0068	0.41	0.16	0.22	0.70
0.88	0.94	6.45	0.0100	0.0094	0.44	0.16	0.23	0.88
1.22	0.91	8.55	0.0111	0.0120	0.52	0.17	0.24	1.22

TABLE XII. $\langle M_{\text{inv}}^{\pi^+\pi^-} \rangle$ asymmetries, $\eta^{\pi^+\pi^-} > 0$, cone cut 0.4

$\langle M_{\text{inv}}^{\pi^+\pi^-} \rangle$	$\langle \sin \theta \rangle$	$\langle p_T^{\pi^+\pi^-} \rangle$ [GeV/c]	$A_{\text{UT}}^{\sin \phi}$	$\sigma_{A_{\text{UT}}^{\sin \phi}}$	$\langle z \rangle$	$\langle x_1 \rangle$	$\langle x_2 \rangle$	$\langle \eta^{\pi^+\pi^-} \rangle$
0.36	0.95	4.73	0.0054	0.0101	0.38	0.23	0.16	0.51
0.50	0.95	5.31	0.0176	0.0067	0.39	0.22	0.16	0.50
0.70	0.96	5.60	0.0183	0.0068	0.42	0.22	0.15	0.50
0.88	0.94	6.45	0.0311	0.0095	0.44	0.22	0.16	0.50
1.22	0.91	8.55	0.0330	0.0119	0.53	0.24	0.17	0.49

TABLE XI. $p_T^{\pi^+\pi^-}$ asymmetries, $\eta^{\pi^+\pi^-} > 0$, cone cut 0.4

$\langle p_T^{\pi^+\pi^-} \rangle$ [GeV/c]	$\langle \sin \theta \rangle$	$\langle M_{\text{Inv}}^{\pi^+\pi^-} \rangle$	$A_{\text{UT}}^{\sin \phi}$	$\sigma_{A_{\text{UT}}^{\sin \phi}}$	$\langle z \rangle$	$\langle x_1 \rangle$	$\langle x_2 \rangle$	$\langle \eta^{\pi^+\pi^-} \rangle$
3.60	0.99	0.53	0.0129	0.0084	0.29	0.20	0.14	0.46
4.48	0.97	0.60	0.0059	0.0073	0.35	0.21	0.15	0.56
5.67	0.94	0.68	0.0246	0.0073	0.42	0.22	0.15	0.56
7.17	0.92	0.76	0.0096	0.0100	0.50	0.23	0.16	0.51
10.28	0.88	0.89	0.0526	0.0099	0.58	0.27	0.19	0.51

TABLE XIII. $\eta^{\pi^+\pi^-}$ asymmetries, cone cut 0.2

$\langle p_T^{\pi^+\pi^-} \rangle$ [GeV/c]	$\langle \sin \theta \rangle$	$\langle M_{\text{Inv}}^{\pi^+\pi^-} \rangle$	$A_{\text{UT}}^{\sin \phi}$	$\sigma_{A_{\text{UT}}^{\sin \phi}}$	$\langle z \rangle$	$\langle x_1 \rangle$	$\langle x_2 \rangle$	$\langle \eta^{\pi^+\pi^-} \rangle$
6.30	0.93	0.50	0.0010	0.0079	0.46	0.15	0.25	-0.7
6.30	0.94	0.50	0.0054	0.0080	0.41	0.18	0.20	-0.2
6.30	0.94	0.50	0.0148	0.0080	0.43	0.21	0.17	0.2
6.30	0.93	0.50	0.0280	0.0079	0.45	0.26	0.15	0.7

TABLE XIV. $\eta^{\pi^+\pi^-}$ asymmetries, cone cut 0.3

$\langle p_T^{\pi^+\pi^-} \rangle$ [GeV/c]	$\langle \sin \theta \rangle$	$\langle M_{\text{Inv}}^{\pi^+\pi^-} \rangle$	$A_{\text{UT}}^{\sin \phi}$	$\sigma_{A_{\text{UT}}^{\sin \phi}}$	$\langle z \rangle$	$\langle x_1 \rangle$	$\langle x_2 \rangle$	$\langle \eta^{\pi^+\pi^-} \rangle$
6.04	0.94	0.59	-0.0002	0.0060	0.45	0.15	0.24	-0.75
5.99	0.94	0.60	0.0075	0.0061	0.40	0.18	0.20	-0.26
5.99	0.94	0.60	0.0131	0.0061	0.42	0.20	0.17	0.26
6.04	0.94	0.59	0.0311	0.0060	0.44	0.25	0.15	0.75

TABLE XV. $\eta^{\pi^+\pi^-}$ asymmetries, cone cut 0.4

$\langle p_T^{\pi^+\pi^-} \rangle$ [GeV/c]	$\langle \sin \theta \rangle$	$\langle M_{\text{Inv}}^{\pi^+\pi^-} \rangle$	$A_{\text{UT}}^{\sin \phi}$	$\sigma_{A_{\text{UT}}^{\sin \phi}}$	$\langle z \rangle$	$\langle x_1 \rangle$	$\langle x_2 \rangle$	$\langle \eta^{\pi^+\pi^-} \rangle$
5.84	0.95	0.67	-0.0027	0.0053	0.44	0.14	0.24	-0.75
5.78	0.95	0.67	0.0074	0.0053	0.40	0.17	0.20	-0.26
5.78	0.95	0.67	0.0095	0.0053	0.41	0.20	0.17	0.26
5.84	0.95	0.67	0.0297	0.0053	0.43	0.24	0.14	0.75